Biomedical Signal Processing and Control 87 (2024) 105411

Contents lists available at ScienceDirect

Biomedical Signal Processing and Control

journal homepage: www.elsevier.com/locate/bspc

EEG-based emotion recognition for road accidents in a simulated driving environment

Jielin Chen *, Xuefen Lin, Weifeng Ma, Yuchen Wang, Wei Tang

School of Information and Electronic Engineering, Zhejiang University of Science and Technology, Hangzhou 310023, People's Republic of China

ARTICLE INFO

Keywords:
EEG classification
Graph neural network
Signal processing
Driving simulation

ABSTRACT

Encountering unexpected events with different levels of danger can cause different levels of emotional changes in the driver, and identifying the driver's mental state can assist in determining whether he or she can control the vehicle. Electroencephalogram (EEG) is an essential component of the basis for emotional classification. Current driving-related EEG research has focused chiefly on fatigue driving and road rage. In order to explore the connection between panic emotion and accident-avoidance ability, this paper proposes an EEG acquisition and emotion classification scheme in a simulated driving environment. The scheme uses vehicle speed as a variable to simulate obstacle avoidance at different danger levels. It uses graph neural networks (GNN) with functional connectivity and attention mechanisms to simulate the physiological structure of the brain to process the data. In addition, various experiments were conducted to compare the features from entropy and power perspectives. The three-class classification result reached 75.26%, with a single label's highest F1 score of 76.7%. The binary classification result reached 91.5%, with a single label's highest F1 score of 91.86%. The experimental results show that the solution can effectively simulate different dangerous situations, capture the driver's EEG signals, and effectively monitor the emotional state in combination with deep learning models.

1. Introduction

With the increasing demand for active safety and intelligence in the automotive market, the substantial social and economic value of intelligent driving is becoming increasingly evident. Statistics show that most traffic accidents are caused by human errors [1], and research on more automated assisted driving systems can help reduce human errors. The concept of ADAS (Advanced Driver Assistance Systems) was first introduced in the 1950s with the application of the anti-lock braking system (ABS) [2]. With subsequent developments, ADAS provides functions such as automatic lighting control, lane change, and adaptive cruise control [3]. On the other hand, some experimental models can achieve highly autonomous driving behaviors through environmental awareness, such as starting, accelerating, braking, lane line tracking, lane changing, obstacle avoidance, and parking. Automated driving is generally divided into five levels, from low to high vehicle autonomous driving capabilities gradually. However, most of the models currently on sale are still in the combined function assistance stage (Level 2), which can complete the essential operation of the vehicle. At the same time, the driver is responsible for peripheral monitoring and taking over the vehicle at any time. The driver is still an essential part of controlling the vehicle, Koohestani et al. [4] demonstrated the importance of collecting various types of information to determine driver status.

In the actual driving process, the driver's emotional state often affects his or her judgment ability and operational accuracy in the face of unexpected events. Negative emotions, such as anger and panic, are common in people's daily lives. When negative emotions occur, people tend to have various abnormal behaviors. Such emotions trigger dangerous behavior and loss of regular judgment while driving. Therefore, collecting driver emotion signals can help the assisted driving system better to determine the driver's emotional state and responsiveness and adjust the intervention timing and strategy based on this information. For example, when the driver is in a mild state of panic, the intensity of assistance is reduced to avoid interfering with the driver's control of the vehicle, thus improving driving comfort. When the driver is in a more severe state of panic, the assisted driving system intervenes in time to avoid accidents.

The signals reflecting the driver's emotions are mainly non-physiological and physiological. Facial expressions, as one of the non-physiological signals, can easily lead to unclear or incorrect signal acquisition due to the different levels of expression of emotions conveyed by different people's faces or influences such as ambient light and shooting angles inside the vehicle. Eliminating such human interference is an additional challenge that will be faced by emotion recognition based on non-physiological signals. In contrast, physiological signals

* Corresponding author.
E-mail address: 222108855034@zust.edu.cn (J. Chen).

https://doi.org/10.1016/j.bspc.2023.105411
Received 23 June 2023; Received in revised form 23 August 2023; Accepted 12 September 2023
Available online 22 September 2023
1746-8094/© 2023 Elsevier Ltd. All rights reserved.

are spontaneously generated by the nervous and endocrine systems [5]. They are not susceptible to human and environmental factors, making them a more diverse and accurate reflection of emotions and a more effective judgment basis [6]. EEG signals, as physiological signals, have millisecond temporal resolution, allowing them to capture the rapid changes that occur in the brain in a short period. In addition, the non-invasive acquisition method does not cause harm to the driver, and the lower acquisition cost facilitates the widespread use of the device.

Different states of brain activity correspond to different levels of neural tissue discharging in each brain region. In general, EEG regions are divided into different regions, such as frontal, parietal, temporal, and occipital lobes, and the electrical signals in different regions are measured by placing electrodes on the surface of the scalp [7]. The convolutional neural network (CNN), in which each convolutional kernel focuses on only a portion of the input, can capture local features and be applied earlier to study EEG signals. However, CNN can only handle grid data, and representing the 3D spatial location of each electrode of the EEG cap by a 2D tensor can cause a large loss of information [8]. Neurons and synapses in the brain are organized in graph structures, which can be considered a non-Euclidean space and do not satisfy translation invariance. Some studies have used graph neural network (GNN) to simulate information transfer between different brain regions [9], showing the advantages of GNN in processing EEG signals. Normal human spontaneous EEG generally ranges from 0–75 μV. EEG generated by induction is weaker than spontaneous EEG, generally in the range of 2–10 μV, and is usually buried in spontaneous potentials and requires feature extraction [10]. Commonly used EEG features can be classified into two categories: entropy [11,12] or power [13,14] and can be divided into five frequency bands: delta (0.5–4 hz), theta (4–8 hz), alpha (8–13 hz), beta (13–30 hz) and gamma (30–100 hz). In this paper, GNN, combined with entropy and power features, will be used to analyze the EEG emotion data in driving scenarios.

Most currently open datasets of EEG emotions are induced by pictures, music, or video clips [7], and much of the driving-related research has focused on areas such as driver fatigue [15] and road rage [16]. In order to study drivers' emotional changes when encountering road emergencies, we need to build a simulated driving scenario that is sufficiently reductive to collect EEG signals from subjects.

In this paper, a simulated driving scenario is built to collect EEG signals from drivers and analyze them using GNN. The simulated driving scenario is implemented by combining a virtual scene and a simulated driver's seat, where the subject and the virtual vehicle are interactable throughout the entire process in compliance with the requirements of the experimental operation. The experiment aims to induce different intensities of panic emotions in subjects using scenarios where the vehicle rushes towards an obstacle at different speeds. On the other hand, we will use an extended graph attention network to test the effect of classifying panic levels with two features: differential entropy (DE) and power spectral density (PSD). While mining the signal features collected by individual EEG electrodes, we will use the graph structure data to simulate the brain topology, and analyze the signal transmission between different brain regions, thus improving classification accuracy.

In summary, the main contributions of this paper are as follows:

1. A simulated driving scenario was constructed that can be applied to a variety of tests, and allows for the acquisition of EEG signals from subjects for research purposes.
2. An experimental protocol is proposed to induce EEG signals from drivers in a simulated environment to analyze their emotional changes when they encounter unexpected events.
3. Multiple tasks are designed to compare the performance of different models in this paper, and the feasibility of using the signals collected in this paper as a basis for determining the driver's emotional state is demonstrated.

2. Related work

2.1. Driving and emotion

Russell et al. [17] showed that human emotional dimensions are not independent, and multiple emotions can be highly systematically expressed in a coordinate system. The model they proposed was widely used in assessing emotions in professionals and laypersons and EEG emotion research. It is worth noting that tired and sleepy are also among the emotional concepts defined by the model. Driving fatigue detection belongs to the more established directions of applying EEG signals to driver affect analysis: Lal et al. [15] earlier summarized the association between driver fatigue and the delta and theta frequency bands of EEG signals. The SEED-VIG dataset [18], an extension of the work on the SEED dataset [11,19], has been widely used in EEG models for testing driving fatigue, a work that inspired the present study was Wang et al. [20] who used this dataset to test their proposed PLI-GAT model and achieved an accuracy of 85.53% in identifying driving fatigue by using GNN combined with functional connectivity.

Several studies have attempted to explore the broader link between driving and emotion: Fan et al. [21] argued that other emotional states of the driver besides fatigue also significantly impact driving behavior and earlier used Bayesian networks to detect driver emotion. Notably, the study considered the effect of traffic conditions on driver emotions and suggested the feasibility of EEG emotion detection to provide adaptive driving assistance. Thirunavukkarasu et al. [22] similarly proposed that an in-vehicle diagnostic system could be combined with a customized intelligent human–machine interface to improve driving safety by analyzing driver emotions. At the same time, they used support vector machine (SVM) to evaluate EEG signal classification in their study. The above research is based on machine learning. Thanks to the progress of computer hardware, the training and inference speed of deep learning has been significantly improved, allowing experimenters to build more extensive and complex models [23–25]. Without restricting data acquisition to simulated driving environments, there is a relatively complete line of development for classification model design using commonly induced EEG emotion data. As an early deep learning model applied to EEG emotion classification, CNN has the advantage that its ability to process more than 2D data provides researchers with the opportunity to increase functional connectivity in the brain. Moon et al. [26] tested the effect of multiple functional connectivities using a modified CNN. A study by Zhao et al. [27] tested the effect of more dimensional raw EEG features on CNN processing of emotion classification tasks, and the study by Liu et al. [28] added attention mechanism to multidimensional features to improve the model.

2.2. Graph neural network

The nodes of graph structure data are arranged in non-Euclidean space, which cannot use fixed-size convolution kernels to extract features of each pixel as CNN does. The essence is to find learnable convolution kernels applicable to graphs and apply tasks such as node classification, edge prediction, and graph classification according to different scenarios. With the development of GNN, two primary operations have been generated: frequency domain convolution and spatial domain convolution, with the main difference being whether the Fourier transform is performed before passing and updating the node information.

The frequency domain convolution model was first proposed by Bruna et al. [29], aiming to derive its Laplace operator in the frequency domain using the Laplace matrix of the graph and to derive a formula for the convolution of the graph by analogy with the convolution of data arranged in Euclidean space in the frequency domain, that is, to update the information of the graph using frequency domain multiplication instead of spatial domain convolution. Let the adjacency

matrix and degree matrix of the graph be A and D, respectively, and the Laplace matrix L can be obtained and decomposed:

$$D_{ii} = \sum_j A_{ij} \tag{1}$$

$$L = D - A = U\Lambda U^{-1} = U\Lambda U^T \tag{2}$$

Let a and b be the convolution kernel and eigenfunction, respectively, then the frequency domain convolution formula of the graph can be expressed as:

$$o = U(U^T a \odot U^T b) \tag{3}$$

Where $U^T a$ can be considered as a learnable convolutional kernel, Defferrard et al. [30] avoided eigenvalue decomposition by using Chebyshev polynomials to approximate the convolutional kernel function, and Kipf et al. [31] further improved the efficiency of the model by taking only the first order of the Chebyshev K-order. In applying EEG-based emotion classification tasks, Song et al. [32] improved the graph convolutional network (GCN) using a dynamically changing graph structure instead of a predefined one. On the other hand, Zhong et al. [33] proposed two regularization methods to improve the cross-subject classification of frequency domain convolution.

Spatial domain convolution is closer to how convolution is applied in CNN, where the core lies in aggregating information from neighboring nodes. The form of spatial domain convolution was first defined by the message-passing neural network [34], which mainly consists of two steps: message passing and state updating. There exist multiple variants of spatial domain convolution that satisfy this framework, such as GraphSAGE [35], GAT [36], and GIN [37]. Moreover, since the Fourier transform of the graph relies on the symmetric semi-positive definite property of the Laplace matrix, frequency domain convolution is only suitable for processing undirected graphs. In contrast, spatial domain convolution is not subject to this limitation. Wang et al. [38] added partial directed coherence to dense graphs to build an EEG emotion classification model. Jang et al. [39] constructed a multilayer graph structure by combining feature fusion with spatial convolution and achieved better classification results than manually defined EEG connectivity structures.

3. Methods

3.1. Building driving scenarios

In order to simulate the scenario of encountering an accident at different speeds in an actual driving environment, a simulated driving system was built for collecting EEG information. The subject sits in front of a large screen and controls the vehicle in the software with a steering wheel and pedals on the seat, and the scenario changes to match the vehicle's movement. Subjects will maintain a straight line as they increase their speed but will encounter an abrupt curve after reaching a set top speed, intended to induce emotional change.

3.1.1. Test track

The test track was divided into three main sections. The first straight section is 100 m long, giving the subject sufficient length to accelerate the vehicle to the different top speeds the experiment requires. The second straight section is 100 m long, during which the subject will maintain a constant speed to simulate a situation where the driver observes an unexpected event with the naked eye but has not yet encountered it. In the third section of the road, the subject will enter an obstacle course to simulate the driver's encounter with an unexpected event at different speeds.

The third section of the road was built based on an evasive maneuver test initially proposed in Sweden. The evasive maneuver test is designed to test the emergency performance of a vehicle while driving to avoid a sudden obstacle in front of it, such as a large wild animal like a moose, hence the name moose test. The test has now been standardized in ISO 3888-2. When entering the moose test section, the subject should cut off the brakes and throttle, quickly change lanes to the opposite lane to avoid the obstacle, and immediately return to the original lane to avoid obstructing oncoming traffic. Generally, a car with excellent emergency performance can pass the moose test at an average speed of 70–80 km/h. The specific test section setup is shown in Fig. 1 and Table 1.

Table 1
The specific sizes (m) of each part of the virtual scene map.

Section	Length	Width
Accelerating	100	1.1 * vehicle width + 0.25
Constant speed	100	1.1 * vehicle width + 0.25
1	12	1.1 * vehicle width + 0.25
2	13.5	–
3	11	vehicle width + 1
4	12.5	–
5	12	1.3 * vehicle width + 0.25, but not less than 3
6	–	1

3.1.2. Other parameters

The vehicle simulation hardware is Logitech G923 TRUEFORCE, which has a steering wheel that supports 900 degrees of rotation better to simulate the steering ratio of a family car. The steering wheel uses a Hall-effect steering sensor, less prone to error input than a potentiometer in a vibrating environment. Dual-motor force feedback enables access to rich environmental information through both hands while the subject is focused on on-screen information. In addition, the entire simulated driving environment is built according to a left-hand drive vehicle.

The vehicle simulation software is Assetto Corsa, which uses a detailed physics engine to provide a realistic driving experience while supporting a wide range of third-party expansion modules. In this experiment, the simulated driving scenario was built using Blender and imported into Assetto Corsa. To avoid redundant operations interfering with the experimental process and keep the subject's driving experience close to a current family car, the environmental simulation parameters were: 1 p.m., clear weather with no wind, ambient temperature 26 °C, and optimal road conditions. The vehicle simulation parameters were: automatic gearbox off, automatic clutch on, automatic throttle blip on, ideal driving line off, traction control on, ABS on, stability control on to 100%, fuel consumption and mechanical damage off. The vehicle selected for testing was a BMW M3 E30 GROUP A with a body width of 1.68 m and a top speed of 50 km/h, 75 km/h and 100 km/h for the first three gears of the gearbox.

3.2. Data preprocessing

As show in Fig. 2, we first checked the EEG signals visually to remove heavily contaminated EEG recordings. Then the whole-brain signal is re-referenced based on M1 and M2 bilateral mastoid signals, electrooculogram (EOG) artifacts in the signal are removed using principal component analysis, and finally, the signal is bandpass filtered from 0.5 to 45 Hz. Due to the different times that have taken to pass through the complete test track at different vehicle speeds, to maintain a consistent length of data input to the model, each segment of the recordings will be cut, mainly retaining the EEG signals from the moose test section. After preprocessing, each subject recorded 30 segments of 18 s in duration, of which the first 3 s were the reference EEG signal in the calm state, and the last 15 s were divided into 3 s of non-overlapping signals for feature extraction. Eventually, each subject contained 150 records and was labeled with equal amounts of the three types of labels. All data preprocessing was done in ASA and Matlab software.

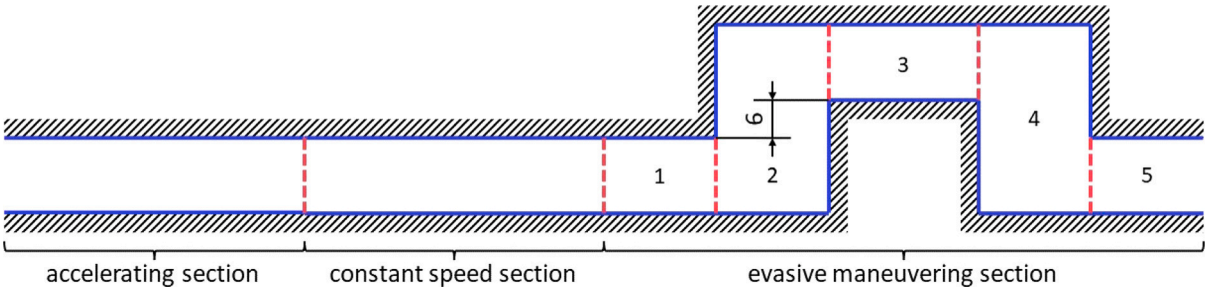

Fig. 1. The map of the virtual scenario used during the subject's test, with the driving direction from left to right.

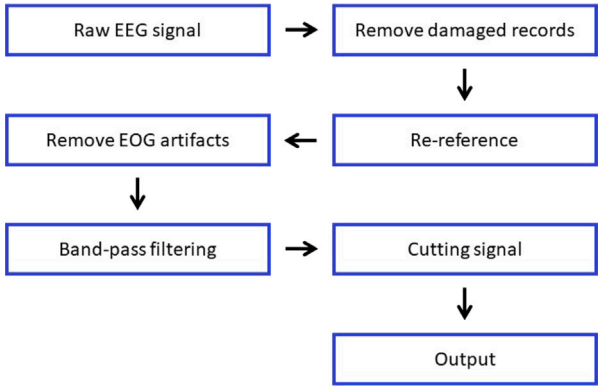

Fig. 2. Data preprocessing process.

3.3. Feature extraction

3.3.1. Differential entropy

The early definition of entropy was mainly for discrete signals. However, in real systems, it is primarily continuous signals, for example, human heart rate signals [40]. Since the entropy of continuous variables is infinite, there is a need to better distinguish the amount of information contained in different continuous random variables in the real system, so the definition of DE is promoted based on Shannon's entropy [11]. DE is widely used as a feature in various types of emotion classification studies. Let X be a continuous random variable with probability density function $p_X(x)$, the DE $E_X(x)$ can be defined as:

$$E_X(x) = -\int_S p_X(x)\log(p_X(x))\mathrm{d}x \tag{4}$$

$$S = \{x \in X \mid p_X(x) > 0\} \tag{5}$$

When X follows a normal distribution:

$$p(x) = \frac{1}{\sqrt{2\pi\sigma^2}}\exp(-\frac{(x-\mu)^2}{2\sigma^2}) \tag{6}$$

The DE can be expressed as:

$$E_X(x) = \frac{1}{2}\log(2\pi e\sigma^2) \tag{7}$$

3.3.2. Power sprctral density

According to the integration of the signal in time:

$$E_{sig} = \int_{-\infty}^{+\infty} sig_{(t)}^2\mathrm{d}t \tag{8}$$

Where E_{sig} represents the integration of the signal in a certain time range and $sig_{(t)}$ represents the signal. Generally, the signal is divided into energy and power signals, where the energy signal has a finite integration over an infinite time, and the power signal has an infinite integration over an infinite time. In scenarios where the energy is concentrated in a finite time interval, the use of the energy spectral density enables to describe the distribution of the signal's energy with frequency:

$$\mathrm{ESD} = |\int_{-\infty}^{+\infty} sig_{(t)}e^{-j2\pi ft}\mathrm{d}t|^2 \tag{9}$$

Where f represents the frequency of the signal. For continuous signals, the PSD must be defined to describe the distribution of the power of the signal or time series with frequency [41].

$$\mathrm{PSD} = \lim_{t\to\infty}\frac{\mathrm{ESD}}{t} \tag{10}$$

Where t represents the time span over which the signal lasts. The actual acquired EEG signal contains a large amount of noise even after preprocessing, resulting in a non-converging Fourier transform of the obtained random signal, and the PSD of the EEG signal is usually used as an analytical feature.

3.3.3. Phase lag index

Normal higher cognitive functions of the brain rely on the synergistic work between different brain regions, and graph structure data can more intuitively preserve the information of each brain region. In order to simulate the association between different brain regions during the experiment, this paper introduces functional connectivity as edge features of the graph. Ideally, each electrode on the EEG cap records only the signal generated directly below it. However, the actual location of signal generation exists at a certain distance from the scalp. Brain tissue disperses cortical neuronal activity to different locations on the scalp, and each electrode picks up signals from adjacent brain regions, i.e., volume conduction effects. Since the electrodes of non-invasive EEG acquisition devices are distributed on the scalp's surface, the volume conduction effect cannot be avoided. This paper uses the phase lag index (PLI) as a functional connectivity index. Stam et al. [42] proposed phase-based functional connectivity for determining the degree of phase synchronization between different channels of EEG signals or magnetoencephalogram (MEG) signals:

$$\mathrm{PLI} = |\langle\mathrm{sign}(\Delta\phi_{rel}(t))\rangle| = |\frac{1}{N}\sum_{n=1}^{N}\mathrm{sign}(\Delta\phi_{rel}(t_n))| \tag{11}$$

Where the sign function outputs 1, −1, and 0 for positive, negative, and 0 inputs, respectively, $\Delta\phi_{rel}$ represents the phase difference between two signals at time point t. PLI takes values in the range [0, 1], and larger values represent a higher degree of synchronization of the signals. In contrast to the functional connectivity PLV [43], which is also based on phase, PLI has the advantage of being insensitive to volume conduction effects and is, therefore, more suitable as an edge feature for the graph structure in this paper.

3.4. Model settings

The specific model structure is shown in Fig. 3. The upper part of Fig. 3 represents the computation process of information within a single node, and the lower part represents the computation process of the whole graph. The data of each EEG channel is input separately

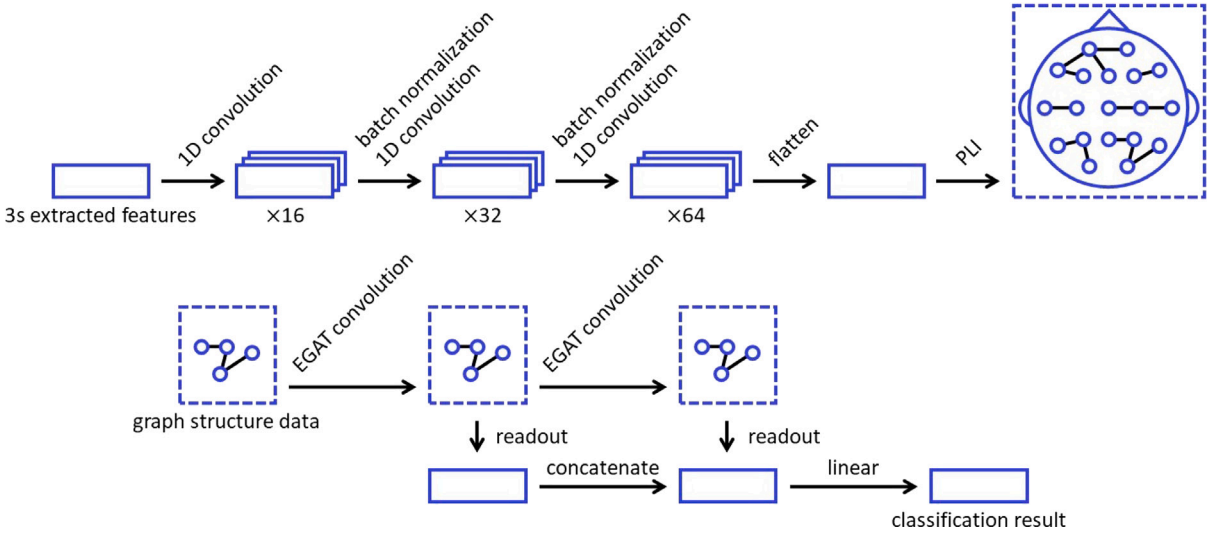

Fig. 3. The overall structure of the deep learning model used in this paper, the output of the first line is the input of the second line.

Fig. 4. The specific experimental scenario.

into a 1D convolution layer to extract the intra-channel features, and then the graph is constructed according to the spatial arrangement of electrodes, and PLI is used as the edge weight of the graph. Each record corresponds to a graph. The graph will be used as input to the GNN, which contains two layers of graph convolution layers, each of which will perform graph readout to obtain graph representations of different depths. The graph representations of each layer will be concatenated to serve as a basis for classification.

The signal within a single EEG channel approximates a time series after preprocessing, so the part extracting the features within the channel uses 1D convolution. The EEG signals of multiple channels are arranged in non-Euclidean space during the construction of the graph, which requires the use of GNN nodes to preserve the data of different electrodes. In addition, to store PLI in the model, we finally choose the graph attention network with edge weights (EGAT) to form the layers of GNN. EGAT is an extension of GAT, which retains the attention mechanism and can better model the information transfer between different brain regions [44]. The computational process of EGAT can be expressed as:

$$f'_{ij} = \mathrm{LeakyReLU}(W[h_i \| f_{ij} \| h_j]) \tag{12}$$

$$e_{ij} = \vec{F} \cdot f'_{ij} \tag{13}$$

$$\alpha_{ij} = \mathrm{softmax}_i(e_{ij}) \tag{14}$$

$$h_i^{(l+1)} = \sum_{j \in M} \alpha_{ij} W^{(l)} h_j^{(l)} \tag{15}$$

where f'_{ij} and f_{ij} represent the edge features before and after calculation, respectively, W and $\vec{F}$ represent the weight matrix and weight vector, respectively, h_i and h_j represent the features of nodes i and j, respectively, e_{ij} and α_{ij} represent the unnormalized and normalized attention scores, respectively, and M represents the number of neighboring nodes of node i.

4. Experiments

4.1. Stimuli

In this paper, three speeds were used to induce different types of emotions: 50 km/h for the urban driving scenario, where subjects had sufficient time to judge and avoid the unexpected situation, and 75 km/h for the suburban driving scenario, which was the limit of the vehicle passing the moose test. At the speed of 75 km/h, the subjects will generate stronger emotions, but most can still avoid the accident. The 100 km/h speed corresponds to a high-speed driving scenario in which the subjects cannot avoid accidents in the simulated environment. At the same time, strong emotional changes occur in the event of an accident.

4.2. Subjects

Ten subjects (5 males and 5 females; mean: 23.40, std: 2.07) with normal or corrected vision and hearing, right-handedness, and with a driver's license participated in the experiment. Subjects were informed about the experimental procedure and practiced using the driving simulator. The distance between the steering wheel and pedals during the experiment was adjusted according to the subject's limb length and driving habits. The subjects were asked to sit comfortably in the simulated driving seat and to start each round of the driving test according to the instructions, as shown in Fig. 4 for the specific experimental scenario. All force feedback and sound playback were designed to recreate the vehicle driving and avoid the subject's unwanted movements and

Table 2
Comparison of the proposed model with different existing studies in average accuracies (%).

Classifier	Features (Dataset)	Classification accuracy
CNN [45]	Raw EEG signals (DEAP)	Valence: 71.00/Arousal:72.00
C-RNN [46]	Continuous wavelet transform (DEAP)	Valence: 72.06/Arousal:74.12
PDC-DGP [38]	Differential entropy (DEAP)	Valence: 77.37/Arousal:76.92
MST based GNN [47]	Continuous wavelet transform (DEAP)	92.31
DGCNN [32]	Differential entropy (SEED)	90.40
RGNN [33]	Differential entropy (SEED)	94.24
P-GCNN [9]	Differential entropy (DEAP)	Valence: 73.31/Arousal: 77.03/Dominance: 79.20
	Rational asymmetry (SEED)	84.35
The present paper	Differential entropy (DEAP)	90.87
	Differential entropy (SEED)	90.22

Table 3
Comparisons of F1 scores (%) for GNN per-label classification.

Tasks	0	1	2
GNN-DE-3class	76.70	66.35	72.13
GNN-PSD-3class	69.16	56.85	63.49
GNN-DE-2class	91.86	–	91.10
GNN-PSD-2class	85.71	–	86.28

Table 4
Comparisons of F1 scores (%) for SVM per-label classification.

Tasks	0	1	2
SVM-DE-3class	68.75	59.57	67.02
SVM-PSD-3class	42.45	37.86	76.19
SVM-DE-2class	78.81	–	91.46
SVM-PSD-2class	61.54	–	71.43

environmental noise interference as much as possible. Subjects were asked to get enough sleep the night before the experiment to ensure a good mental state and adequate agility during the experiment. Before the experiment, subjects were asked to clean all electrodes on the scalp, forehead and behind the ears, ensuring that their hair and scalp were dry before wearing the electrode caps. All subjects participating in the experiment will be paid.

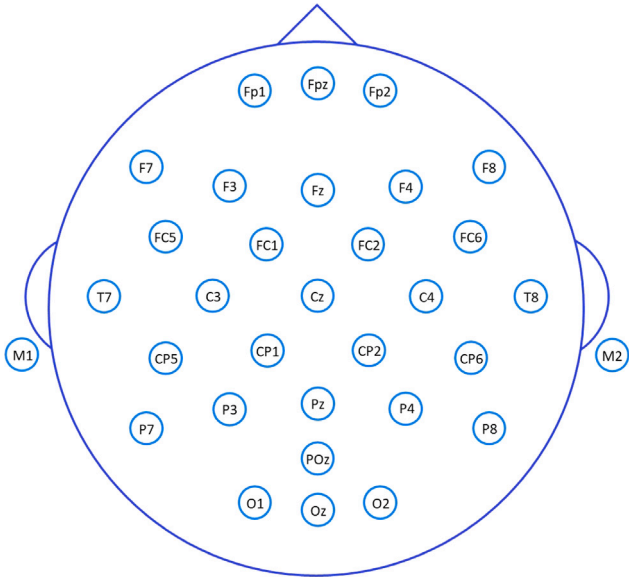

Fig. 5. The electrode placement scheme of the 5% electrode system.

4.3. Protocol

We chose a quiet environment to conduct the experiments in the morning or late afternoon. The electrode placement scheme used was a 5% electrode system, an extension of the international 10–20 and 10-10 systems, using the ANT Neuro eego system to record EEG signals at a sampling frequency of 1000 Hz on a 32-channel EEG cap and keeping the impedance of each electrode within 20 kΩ during the recording process. The distribution of electrodes on the EEG cap is shown in Fig. 5, where the signals acquired from M1 and M2 bilateral mastoid electrodes were not included in the final analysis data. Each subject performed 30 trials. A 5-second cue preceded each trial, and sufficient rest time was provided to start the subsequent trial when the subject was cued to be ready.

4.4. Experiment results

As shown in Table 2, we tested the model performance using DEAP and SEED, two widely used publicly available datasets in the field of EEG emotion research, before inputting EEG data from a simulated driving environment. DEAP dataset contains 32 subjects (16 males and 16 females, mean age 26.9 years), each subject's emotion was induced by 40 music video clips. SEED dataset contains 15 subjects (7 males and 8 females, mean age 23.27 years), each subject's emotion was induced by 15 video clips approximately 4 min long. As shown in studies 1–2, the model proposed in this paper shows better performance than the improved CNN. Studies 3–7 in the table list current representative GNN models, and the model in this paper is close to the best performance among them. It is worth noting that Liu et al.'s study used only the most emotionally informative signal segments, while Zhong et al. reassigned labels to the dataset. This paper did not optimize the model for the dataset for testing purposes.

This paper contains two tasks to test the classification effect of the model, and the main difference is the number of labels for classification. The labels are set according to the different vehicle speeds in the experiment, and the data induced at 50 km/h, 75 km/h and 100 km/h speeds are labeled as "0", "1", and "2 ". All data were used for the three-class classification, and data labeled "0" and "2" were selected for the binary classification. This paper uses two representative models to test the data: the model for deep learning uses a GNN composed of EGAT, the specific structure of which has been described in Section 3.4. and the model for machine learning chooses an SVM widely used in EEG emotion classification. We ensured all models were trained and tested using the same data partitioning process. Precisely 20% of the data were randomly selected as the test set, and the rest of the data were used as the training and validation sets, so all the results below are the means of the 5-fold cross-validation.

Tables 3 and 4 show the classification effect of each label when using the full band of EEG signals. We use the F1 score as an evaluation metric for individual labels, which serves as a reconciled average of precision and recall and can take both into account. Given that the four predicted outcomes are true positive cases (TP), false positive cases (FP), false negative cases (FN) and true negative cases (TN), the precision, recall and F1 score are expressed as follows:

$$\text{precision} = \frac{TP}{TP + FP} \tag{16}$$

Table 5
Comparisons of the average accuracies and standard deviations (%) of the GNN using EEG signals in different frequency bands.

Tasks	Delta band	Theta band	Alpha band	Beta band	Gamma band	Full band
GNN-DE-3class	53.47/11.97	46.23/11.38	53.85/9.49	72.64/10.40	75.26/9.84	71.87/10.33
GNN-PSD-3class	43.67/9.38	47.18/9.74	48.33/9.20	64.53/10.43	68.08/10.79	63.27/11.55
GNN-DE-2class	73.25/8.23	74.38/11.97	73.50/9.44	85.47/9.71	90.31/6.67	91.50/6.26
GNN-PSD-2class	62.83/14.18	60.50/9.85	69.45/9.56	79.21/6.58	87.16/8.56	86.00/11.97

Table 6
Comparisons of the average accuracies and standard deviations (%) of the SVM using EEG signals in different frequency bands.

Tasks	Delta band	Theta band	Alpha band	Beta band	Gamma band	Full band
SVM-DE-3class	57.38/10.98	58.46/11.76	60.27/8.43	71.93/9.47	66.12/8.95	65.33/10.26
SVM-PSD-3class	41.52/11.97	53.31/9.81	53.28/8.57	56.74/11.55	57.93/11.31	42.94/10.40
SVM-DE-2class	77.40/11.78	76.56/11.32	77.57/12.25	84.58/10.87	86.18/10.49	84.43/9.95
SVM-PSD-2class	55.16/9.32	67.81/11.12	66.43/11.95	72.92/10.07	73.43/10.55	65.74/11.06

$$\text{recall} = \frac{\text{TP}}{\text{TP} + \text{FN}} \tag{17}$$

$$\text{F1 score} = \frac{2 \times \text{precision} \times \text{recall}}{\text{precision} + \text{recall}} \tag{18}$$

In most cases, DE was able to obtain higher F1 scores when used as a feature, reflecting its superior performance as a classification feature for EEG signals, a result that has been consistently demonstrated in several studies [19,48]. The binary classification task achieved better performance than the three-class classification task, as expected, due to the binary classification feature having a more significant inter-class gap and a smaller number of labels. It is worth noting that comparing the results of Tables 3 and 4, the F1 scores of GNN per-label classification results are closer and do not show an uneven performance per-label classification similar to that of the SVM-PSD-3class task.

Tables 5 and 6 show the classification accuracy and standard deviation at different frequency bands of EEG signals. The results show better performance when using higher frequency bands such as beta or gamma for emotion classification. Using signals in the full frequency band contains richer features but only sometimes results in the best classification results. The difficulty of the classification task, the quality of the features, and the model all affect the results. For example, in the GNN-DE-2class task, the higher quality of the features and the relative simplicity of the task led to the best results for the full-band analysis. In contrast, in other tasks, the use of full-band data introduced more noise and led to a decrease in classification accuracy. In addition, GNN has higher classification accuracy than traditional machine learning models when using beta and above bands or full-band signals and causes less accuracy degradation when encountering complex tasks.

5. Discussion

The confusion matrix in Fig. 6 shows that the classification results of GNN using full band signals, for example, achieved close classification results for labels “0” and “2” in the three-class classification but poor classification results for label “1” in the middle. “1” in the middle of the triple classification task is poor. It is speculated that when avoiding an unexpected event at low speeds, the driver does not produce significant emotional changes due to a sufficient reaction time and can be considered to have complete driving and risk avoidance capabilities. For dangerous high-speed emergencies that are almost unavoidable, the driver’s emotions change dramatically and can signal the need for intelligent driving to assist in avoidance. However, when the vehicle is at the limit of safe avoidance, it is more difficult for drivers with different experiences to determine whether their level of panic has affected vehicle handling. In this case, the blind intervention of assisted driving may cause negative effects.

Again, taking the three-class classification results of GNN using full band signals as an example, Fig. 7 shows the classification accuracy of each subject individually. Since cross-subject sentiment recognition will significantly decrease classification accuracy, this experiment trains the model for each subject individually. However, there are still large individual differences among subjects. In this experiment, the subject with the lowest classification accuracy deviated from the mean value by 9.72%, and the subject with the highest classification accuracy deviated from the mean value by 8.68%. Each driver has different thresholds for emotional changes in the face of unexpected events. Suppose the intelligent car system can learn the owner’s driving patterns and make fine adjustments. In that case, it will provide a more valuable reference for the timing of assisted driving access, thus further improving driving safety.

6. Conclusion

In this paper, we designed an experiment to collect EEG signals from drivers in a simulated driving environment. The experiment analyses the driver’s emotional changes in the face of different emergencies. It provides a basis for determining whether he or she can still control the vehicle within a short period after encountering danger. First, we used speed as a variable to simulate emergencies with different danger levels and preprocessed the collected signals. Second, we designed multiple classification tasks to compare the differences between the two types of features and the performance of common models. Finally, our study demonstrates the scheme’s feasibility in determining the driver’s emotional state by EEG signals.

Cross-subject classification models can be applied to a wider range of application scenarios, and the current cross-subject classification performance of the model in this paper still has limitations, which means that an independent model needs to be trained for each subject. In addition, the EEG captured in this paper uses a 32-electrode EEG cap, which is too costly to use for portable scenarios. We consider trying to reduce the number of EEG channels and incorporate pre-trained models in future work to further improve the model classification efficiency, and on the other hand, improve the cross-subject classification performance of the model.

CRediT authorship contribution statement

Jielin Chen: Conceptualization, Methodology, Writing – original draft. **Xuefen Lin:** Data processing, Writing – review & editing. **Weifeng Ma:** Visualization, Supervision. **Yuchen Wang:** Resources, Supervision. **Wei Tang:** Format proofreading, Content modification.

Declaration of competing interest

The authors declare that they have no known competing financial interests or personal relationships that could have appeared to influence the work reported in this paper.

Data availability

Data will be made available on request.

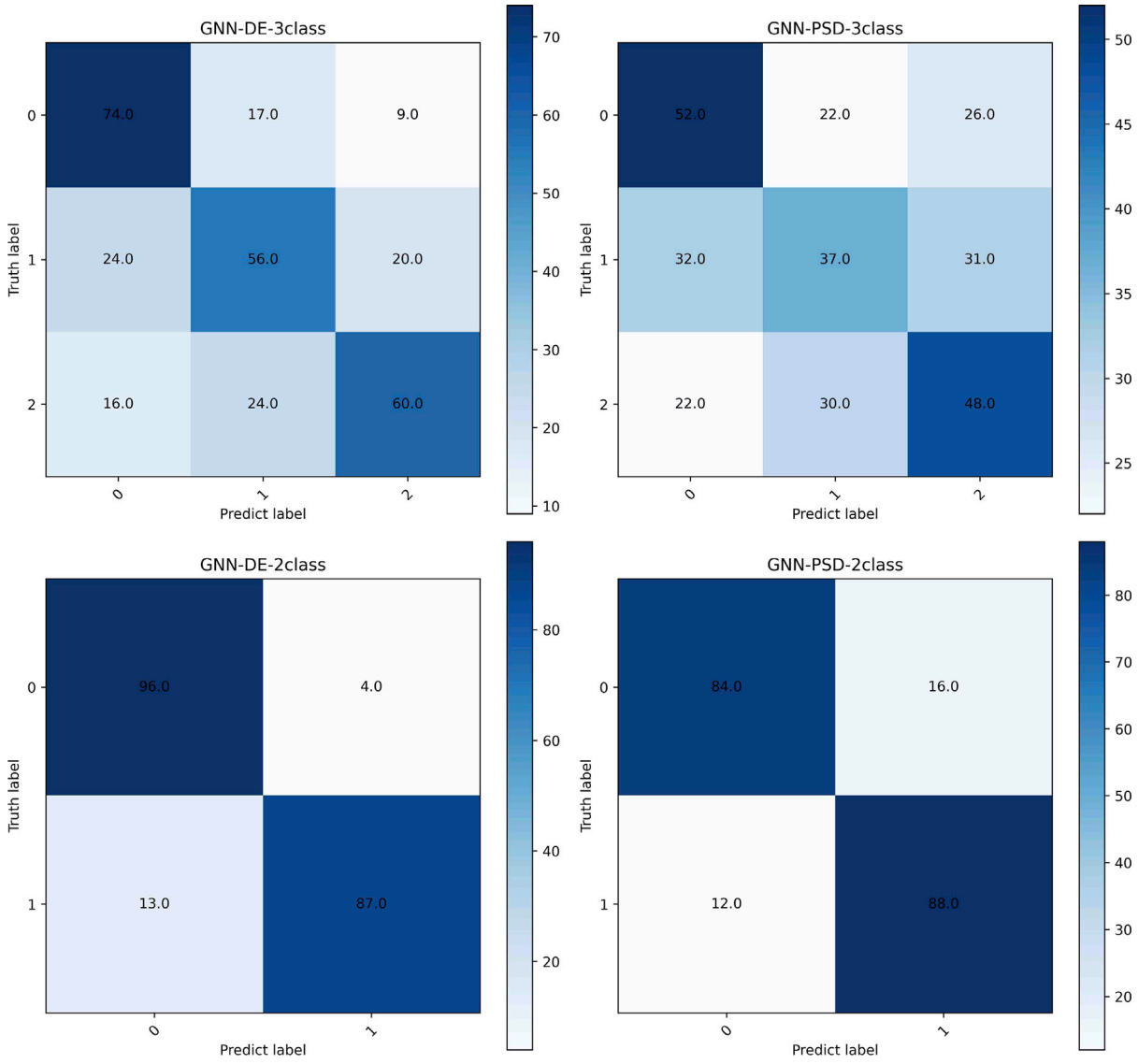

Fig. 6. The confusion matrix of the classification results of GNN using full band signals.

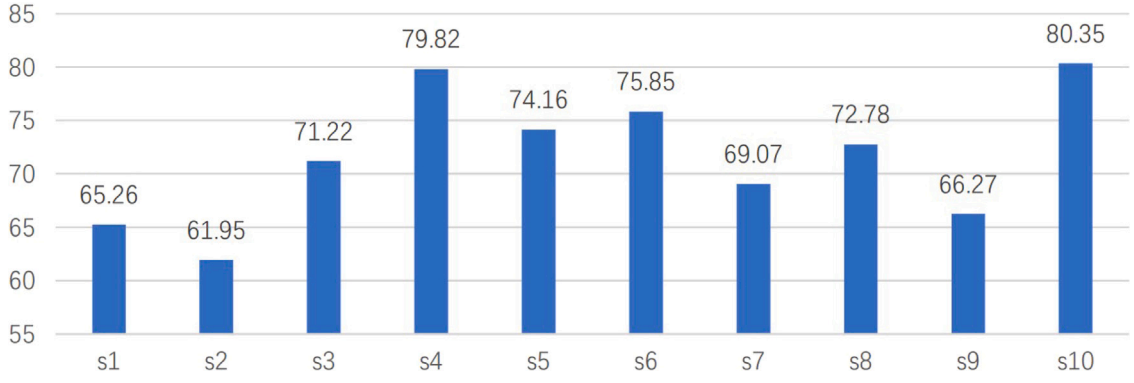

Fig. 7. The classification accuracy (%) of each subject of GNN using full band signals.

References

[1] K.A. Brookhuis, D. De Waard, W.H. Janssen, Behavioural impacts of advanced driver assistance systems–an overview, Eur. J. Transp. Infrastruct. Res. 1 (3) (2001).

[2] M. Galvani, History and future of driver assistance, IEEE Instrum. Meas. Mag. 22 (1) (2019) 11–16.

[3] A. Shaout, D. Colella, S. Awad, Advanced driver assistance systems-past, present and future, in: 2011 Seventh International Computer Engineering Conference (ICENCO'2011), IEEE, 2011, pp. 72–82.

[4] A. Koohestani, M. Abdar, S. Hussain, A. Khosravi, D. Nahavandi, S. Nahavandi, R. Alizadehsani, Analysis of driver performance using hybrid of weighted ensemble learning technique and evolutionary algorithms, Arab. J. Sci. Eng. 46 (2021) 3567–3580.

[5] L. Shu, J. Xie, M. Yang, Z. Li, Z. Li, D. Liao, X. Xu, X. Yang, A review of emotion recognition using physiological signals, Sensors 18 (7) (2018) 2074.
[6] Z. Yin, M. Zhao, Y. Wang, J. Yang, J. Zhang, Recognition of emotions using multimodal physiological signals and an ensemble deep learning model, Comput. Methods Programs Biomed. 140 (2017) 93–110.
[7] M.R. Islam, M.A. Moni, M.M. Islam, M. Rashed-Al-Mahfuz, M.S. Islam, M.K. Hasan, M.S. Hossain, M. Ahmad, S. Uddin, A. Azad, et al., Emotion recognition from EEG signal focusing on deep learning and shallow learning techniques, IEEE Access 9 (2021) 94601–94624.
[8] D. Zhang, L. Yao, X. Zhang, S. Wang, W. Chen, R. Boots, B. Benatallah, Cascade and parallel convolutional recurrent neural networks on EEG-based intention recognition for brain computer interface, in: Proceedings of the Aaai Conference on Artificial Intelligence, Vol. 32, (1) 2018.
[9] Z. Wang, Y. Tong, X. Heng, Phase-locking value based graph convolutional neural networks for emotion recognition, IEEE Access 7 (2019) 93711–93722.
[10] M. Teplan, et al., Fundamentals of EEG mea1surement, Meas. Sci. Rev. 2 (2) (2002) 1–11.
[11] R.-N. Duan, J.-Y. Zhu, B.-L. Lu, Differential entropy feature for EEG-based emotion classification, in: 2013 6th International IEEE/EMBS Conference on Neural Engineering (NER), IEEE, 2013, pp. 81–84.
[12] S.A. Hosseini, M.B. Naghibi-Sistani, Emotion recognition method using entropy analysis of EEG signals, Int. J. Image Graph. Signal Process. 3 (5) (2011) 30.
[13] M. Murugappan, N. Ramachandran, Y. Sazali, et al., Classification of human emotion from EEG using discrete wavelet transform, J. Biomed. Sci. Eng. 3 (04) (2010) 390.
[14] M. Ende, A.K. Louis, P. Maass, G. Mayer-Kress, EEG signal analysis by continuous wavelet transform techniques, in: Nonlinear Analysis of Physiological Data, Springer, 1998, pp. 213–219.
[15] S.K. Lal, A. Craig, A critical review of the psychophysiology of driver fatigue, Biol. Psychol. 55 (3) (2001) 173–194.
[16] X. Gao, C. Xu, Y. Song, J. Hu, J. Xiao, Z. Meng, Node-wise domain adaptation based on transferable attention for recognizing road rage via EEG, in: ICASSP 2023-2023 IEEE International Conference on Acoustics, Speech and Signal Processing (ICASSP), IEEE, 2023, pp. 1–5.
[17] J.A. Russell, A circumplex model of affect, J. Pers. Soc. Psychol. 39 (6) (1980) 1161.
[18] W.-L. Zheng, B.-L. Lu, A multimodal approach to estimating vigilance using EEG and forehead EOG, J. Neural Eng. 14 (2) (2017) 026017.
[19] W.-L. Zheng, B.-L. Lu, Investigating critical frequency bands and channels for EEG-based emotion recognition with deep neural networks, IEEE Trans. Auton. Mental Dev. 7 (3) (2015) 162–175.
[20] Z. Wang, Y. Zhao, Y. He, J. Zhang, Phase lag index-based graph attention networks for detecting driving fatigue, Rev. Sci. Instrum. 92 (9) (2021) 094105.
[21] X.-A. Fan, L.-Z. Bi, Z.-L. Chen, Using EEG to detect drivers' emotion with Bayesian networks, in: 2010 International Conference on Machine Learning and Cybernetics, Vol. 3, IEEE, 2010, pp. 1177–1181.
[22] G.S. Thirunavukkarasu, H. Abdi, N. Mohajer, A smart HMI for driving safety using emotion prediction of EEG signals, in: 2016 IEEE International Conference on Systems, Man, and Cybernetics (SMC), IEEE, 2016, pp. 004148–004153.
[23] W. Wang, Y. Pei, S.-H. Wang, J. manuel Gorrz, Y.-D. Zhang, PSTCNN: Explainable COVID-19 diagnosis using PSO-guided self-tuning CNN, Biocell: Off. J. Sociedades Latinoamericanas De Microscopia Electronica... et. al 47 (2) (2023) 373.
[24] Y. Zhang, L. Deng, H. Zhu, W. Wang, Z. Ren, Q. Zhou, S. Lu, S. Sun, Z. Zhu, J.M. Gorriz, et al., Deep learning in food category recognition, Inf. Fusion (2023) 101859.
[25] W. Wang, X. Zhang, S.-H. Wang, Y.-D. Zhang, Covid-19 diagnosis by WE-SAJ, Syst. Sci. Control Eng. 10 (1) (2022) 325–335.
[26] S.-E. Moon, C.-J. Chen, C.-J. Hsieh, J.-L. Wang, J.-S. Lee, Emotional EEG classification using connectivity features and convolutional neural networks, Neural Netw. 132 (2020) 96–107.
[27] Y. Zhao, J. Yang, J. Lin, D. Yu, X. Cao, A 3D convolutional neural network for emotion recognition based on EEG signals, in: 2020 International Joint Conference on Neural Networks (IJCNN), IEEE, 2020, pp. 1–6.
[28] J. Liu, Y. Zhao, H. Wu, D. Jiang, Positional-spectral-temporal attention in 3D convolutional neural networks for EEG emotion recognition, in: 2021 Asia-Pacific Signal and Information Processing Association Annual Summit and Conference (APSIPA ASC), IEEE, 2021, pp. 305–312.
[29] J. Bruna, W. Zaremba, A. Szlam, Y. LeCun, Spectral networks and locally connected networks on graphs, 2013, arXiv preprint arXiv:1312.6203.
[30] M. Defferrard, X. Bresson, P. Vandergheynst, Convolutional neural networks on graphs with fast localized spectral filtering, in: Advances in Neural Information Processing Systems, Vol. 29, 2016.
[31] T.N. Kipf, M. Welling, Semi-supervised classification with graph convolutional networks, 2016, arXiv preprint arXiv:1609.02907.
[32] T. Song, W. Zheng, P. Song, Z. Cui, EEG emotion recognition using dynamical graph convolutional neural networks, IEEE Trans. Affect. Comput. 11 (3) (2018) 532–541.
[33] P. Zhong, D. Wang, C. Miao, EEG-based emotion recognition using regularized graph neural networks, IEEE Trans. Affect. Comput. 13 (3) (2020) 1290–1301.
[34] J. Gilmer, S.S. Schoenholz, P.F. Riley, O. Vinyals, G.E. Dahl, Neural message passing for quantum chemistry, in: International Conference on Machine Learning, PMLR, 2017, pp. 1263–1272.
[35] W. Hamilton, Z. Ying, J. Leskovec, Inductive representation learning on large graphs, in: Advances in Neural Information Processing Systems, Vol. 30, 2017.
[36] P. Veličković, G. Cucurull, A. Casanova, A. Romero, P. Lio, Y. Bengio, Graph attention networks, 2017, arXiv preprint arXiv:1710.10903.
[37] K. Xu, W. Hu, J. Leskovec, S. Jegelka, How powerful are graph neural networks?, 2018, arXiv preprint arXiv:1810.00826.
[38] Z. Wang, Y. Liu, R. Zhang, J. Zhang, X. Guo, EEG-based emotion recognition using partial directed coherence dense graph propagation, in: 2022 14th International Conference on Measuring Technology and Mechatronics Automation (ICMTMA), IEEE, 2022, pp. 610–617.
[39] S. Jang, S.-E. Moon, J.-S. Lee, Eeg-based emotional video classification via learning connectivity structure, IEEE Trans. Affect. Comput. (2021).
[40] F. Nasirzadeh, M. Mir, S. Hussain, M. Tayarani Darbandy, A. Khosravi, S. Nahavandi, B. Aisbett, Physical fatigue detection using entropy analysis of heart rate signals, Sustainability 12 (7) (2020) 2714.
[41] R.N. Youngworth, B.B. Gallagher, B.L. Stamper, An overview of power spectral density (PSD) calculations, Opt. Manuf. Test. VI 5869 (2005) 206–216.
[42] C.J. Stam, G. Nolte, A. Daffertshofer, Phase lag index: assessment of functional connectivity from multi channel EEG and MEG with diminished bias from common sources, Hum. Brain Mapp. 28 (11) (2007) 1178–1193.
[43] J.-P. Lachaux, E. Rodriguez, J. Martinerie, F.J. Varela, Measuring phase synchrony in brain signals, Hum. Brain Mapp. 8 (4) (1999) 194–208.
[44] K. Kamiński, J. Ludwiczak, M. Jasiński, A. Bukala, R. Madaj, K. Szczepaniak, S. Dunin-Horkawicz, Rossmann-toolbox: a deep learning-based protocol for the prediction and design of cofactor specificity in rossmann fold proteins, Brief. Bioinform. 23 (1) (2022) bbab371.
[45] W. Kristianto, H. Candra, EEG–based emotion classification using convolutional neural networks, in: 2019 2nd International Conference on Applied Engineering (ICAE), IEEE, 2019, pp. 1–4.
[46] X. Li, D. Song, P. Zhang, G. Yu, Y. Hou, B. Hu, Emotion recognition from multi-channel EEG data through convolutional recurrent neural network, in: 2016 IEEE International Conference on Bioinformatics and Biomedicine (BIBM), IEEE, 2016, pp. 352–359.
[47] H. Liu, J. Zhang, Q. Liu, J. Cao, Minimum spanning tree based graph neural network for emotion classification using EEG, Neural Netw. 145 (2022) 308–318.
[48] S. Hwang, K. Hong, G. Son, H. Byun, Learning CNN features from DE features for EEG-based emotion recognition, Pattern Anal. Appl. 23 (2020) 1323–1335.